Study of the Structure, Acidic, and Catalytic Properties of Binary Mixed-Oxide MoO_3−ZrO_2 Systems

Bárbara Samaranch,[†] Pilar Ramírez de la Piscina,*[,†] Guillaume Clet,[‡] Marwan Houalla,[‡] and Narcís Homs*[,†]

Departament de Química Inorgànica, Universitat de Barcelona, C/ Martí i Franquès 1-11, 08028 Barcelona, Spain, and Laboratoire de Catalyse et Spectrochimie (UMR CNRS 6506), ENSICAEN-Université de Caen, 6 Boulevard du Maréchal Juin, 14050 Caen Cedex, France

Received November 4, 2005. Revised Manuscript Received January 27, 2006

Binary mixed-oxide materials based on MoO_3−ZrO_2 (1−68 wt/wt MoO_3 nominal content) were prepared by a sol−gel method. The samples were characterized after calcination at 873 K by X-ray diffraction, Raman, UV−vis, and infrared spectroscopy. An increase in the molybdenum content produces an increase in the surface area up to ca. 140 $m^2\ g^{-1}$ for a nominal MoO_3 content of ca. 20 wt/wt. Simultaneously, the progressive generation of Brönsted acid sites attributed to the presence of surface polymolybdate species takes place. The $Zr(MoO_4)_2$ crystalline phase coexists with polymolybdate species for catalysts with a nominal MoO_3 content higher than 20 wt/wt. These samples show a lower surface area, but the number of Brönsted acid sites per unit of surface area remains almost constant up to ca. 30 wt/wt MoO_3 content. A relationship between the structure of molybdenum surface species, the surface acidity determined by the adsorption of 2,6-dimethylpyridine, and the catalytic behavior of materials in the 2-propanol dehydration are reported.

Introduction

The development of new materials active in acid-catalyzed reactions under mild experimental conditions is a matter of current interest both in academia and in industrial research areas. The use of materials with appropriate acid properties could displace industrial catalytic processes, which use unfriendly acids in the homogeneous phase.[1] The main challenge in this area is to develop solid catalysts with a high density of relatively strong acid sites.

Since the pioneering work of Hino and Arata,[2] it has been well established that zirconia-based binary oxides are promising systems that can exhibit catalytic activity as solid acid catalysts at low temperature. In this context, many studies have been carried out with the goal of developing suitable preparation methods that lead to ZrO_2-based mixed oxides with the appropriate surface properties. This type of catalyst is usually prepared by impregnating zirconium oxyhydroxide with an aqueous solution of an isopolymetalate precursor, followed by drying and calcination. These solids are used as catalysts for various reactions or as supports in the synthesis of bifunctional catalysts.[3−9] Significant interest has been shown for the WO_3−ZrO_2 system. It is believed that strong acid sites are formed by combining tungsten oxide with zirconia present in the tetragonal form.[1] Related systems such as MoO_3−ZrO_2, which exhibits similar properties, have also been examined.[10] It has been shown that the preparation method determines the dispersion and nature of molybdenum species on the surface. These species, in turn, condition the acidity and catalytic properties of the solids. MoO_3−ZrO_2 catalysts prepared by wet impregnation or equilibrium adsorption methods have been widely studied. In this case, the nuclearity of molybdenum species is mostly controlled by the acid−base properties of support sites.[5,11] However, less attention has been paid to the study of MoO_3−ZrO_2 samples prepared via sol−gel methods. These procedures should allow a more uniform distribution of active sites throughout the support material (ZrO_2).[12,13]

The aim of this paper is to obtain more insight into the structural characteristics and the acid nature of MoO_3−ZrO_2 system in relation to its catalytic properties. Solids with a wide range of composition (1−68 wt/wt MoO_3 nominal content) were synthesized by a sol−gel process. To identify the zirconium-containing phases and the molybdenum species present, we analyzed samples by X-ray diffraction, Raman,

* To whom correspondence should be addressed. Tel.: 34-934037056. Fax: 34-934907725. E-mail: narcis.homs@qi.ub.es (N.H.), pilar.piscina@qi.ub.es (P.R.d.l.P.).
[†] Universitat de Barcelona.
[‡] ENSICAEN-Université de Caen.

(1) Corma, A.; Garcia, H. *Chem. Rev.* **2003**, *103*, 4307.
(2) Hino, M.; Arata, K. *Chem. Commun.* **1987**, 1259.
(3) Arata, K. *Appl. Catal., A* **1996**, *146*, 3.
(4) Iglesia, E.; Barton, D. G.; Soled, S. L.; Miseo, S.; Baumgartner, J. E.; Gates, W. E.; Fuentes, G. A.; Meitzner, G. D. *Stud. Surf. Sci. Catal.* **1996**, *101*, 533.
(5) Indovina, V. *Catal. Today* **1998**, *41*, 95.
(6) Fitzsimons, G.; Clarke, J. K. A.; Smith, M. R.; Rooney, J. J. *Catal. Lett.* **1998**, *52*, 69.
(7) Ono, Y. *Catal. Today* **2003**, *81*, 3.
(8) Vu, T. N.; van Gestel, J.; Wilson, J. P.; Mollet, C.; Dath, J. P.; Duchet, J. C. *J. Catal.* **2005**, *231*, 453.
(9) Arata, K.; Matsuhashi, H.; Hino, M.; Nakamura, H. *Catal. Today* **2003**, *81*, 17.
(10) Hino, M.; Arata, K. *Chem. Lett.* **1989**, 971.
(11) Prinetto, F.; Cerrato, G.; Ghiotti, G.; Chiorino, A.; Campa, M. C.; Gazzoli, D.; Indovina, V. *J. Phys. Chem.* **1995**, *99*, 5556.
(12) Koc, S. N.; Gürdag, G.; Löffler, E.; Orbay, M.; Muhler, M. *Mater. Chem. Phys.* **2004**, *86*, 315.
(13) Koc, S. N.; Gürdag, G.; Geissler, S.; Guraya, M.; Orbay, M.; Muhler, M. *J. Mol. Catal. A: Chem.* **2005**, *225*, 197.

10.1021/cm052433c CCC: $33.50
Published on Web 02/23/2006

UV−visible, and infrared spectroscopy. The development of acidity on the surface was monitored by the adsorption of 2,6-dimethylpyridine (lutidine), followed by Fourier transform infrared spectroscopy. The results were correlated with the catalytic activity for an acid-catalyzed reaction (2-propanol dehydration) and the molybdenum species on the catalyst.

Experimental Section

Samples were prepared by mixing an aqueous ammonia/propanol solution of $(NH_4)_6Mo_7O_{24}{\cdot}4H_2O$ and a 1-propanol solution of zirconium propoxide; the latter was prepared under an inert atmosphere. Both solutions were added at room temperature to a vessel containing 1-propanol with vigorous external mechanical stirring. The suspension was aged at 343 K for 6 h and then at 298 K for 16 h. The solids were filtered, dried at 383 K, and subsequently calcined in air at 873 K for 4 h. Samples were labeled *x*MoZr, where *x* designates the nominal wt % MoO_3 in the solid.

The BET surface area was determined by nitrogen adsorption at 77 K with a Micromeritics ASAP9000 instrument. The chemical composition of samples was determined using inductively coupled plasma with atomic emission spectroscopy (ICP-AES) in an Optima Perkin-Elmer 3200RL apparatus.

X-ray diffraction (XRD) patterns were recorded with a Siemens D-500 powder X-ray diffractometer equipped with a graphite monochromator and a Cu target. Diffractograms were recorded at a step width of 0.02°. The signal was accumulated for 10 s at each step.

Raman spectroscopy was performed with a Jobin Yvon T64000 instrument using an Ar ion laser as the illumination source (514.5 nm) and a CCD detector cooled to 140 K. The collection optics system was used in the backscattering configuration, and the apparatus was operated in the Macro Raman mode with a resolution better than 2 cm^{-1}. The laser power was 70 mW. Samples were studied in the 20−1200 cm^{-1} range.

Diffuse reflectance UV−vis spectra (DRS) were recorded on a UV-2101 PC Shimadzu spectrophotometer equipped with a diffuse-reflectance accessory. UV−vis spectra were measured in the reflectance mode, using MgO as reference, in the 200−600 nm range.

Fourier transform infrared experiments (FTIR) were carried out with a Nicolet Magna IR550, equipped with a DTGS detector. Infrared spectra were obtained at room temperature at a resolution of 4 cm^{-1} by collecting 128 scans. Samples were pressed into pellets (∼20 mg; 2 cm^2). They were first treated under vacuum at 723 K for 1 h, then in O_2 (P_{O_2} = 13.3 kPa) for 1 h, and finally evacuated for 1 h at 473 K. 2,6-Dimethylpyridine (lutidine) adsorption was carried out at 373 K (P = 133 Pa) followed by thermal desorption from 373 to 523 K under vacuum. The number of Brönsted acid sites titrated by 2,6-dimethylpyridine was calculated using an integrated molar absorption coefficient value of $\epsilon = 6.8$ cm μmol^{-1} for the sum of the ($\nu_{8a} + \nu_{8b}$) vibrations of protonated lutidine at ca. 1640 and 1628 cm^{-1}.[14]

Catalytic conversion of 2-propanol was measured at initial reaction times in a continuous flow glass microreactor at atmospheric pressure and 353 K. Prior to the catalytic test, samples were treated under Ar at 723 K and then cooled to the reaction temperature. The reactant mixture was a feed of argon saturated with 2-propanol vapor, generated by bubbling Ar (90 mL min^{-1}) through a saturator maintained at 273 K ($P_{2-propanol}$ = 1.2 kPa). Mixtures containing 40−100 mg of samples diluted with inactive SiC were used for each of the catalytic tests, yielding a catalyst bed volume of 1 mL. The products were analyzed on-line with a gas chromatograph (VarianStar 3400CX) equipped with a TRACER TRB-1 column and a flame ionization detector.

Table 1. Characteristics of the MoO_3−ZrO_2 Solids Prepared via a Sol−Gel Method and Calcined at 873 K

sample	MoO_3 (wt/wt)	BET surface area ($m^2\ g^{-1}$)	d_{calcd} (Mo_{atom}/nm^2)	phases (XRD)	V_m[a]
0MoZr	0	26	0	ZrO_2(m); ZrO_2(t)	62
1MoZr	1.22	49	1.0	ZrO_2(m); ZrO_2(t)	57
2MoZr	1.52	47	1.3	ZrO_2(m); ZrO_2(t)	56
3MoZr	2.73	39	2.7	ZrO_2(m); ZrO_2(t)	46
6MoZr	5.59	71	3.3	ZrO_2(t)	32
12MoZr	12.49	120	4.3	ZrO_2(t)	
15MoZr	15.01	143	4.4	ZrO_2(t)	
16MoZr	15.65	131	5.0	ZrO_2(t)	
17MoZr	17.25	137	5.3	ZrO_2(t)	
19MoZr	18.79	126	6.2	ZrO_2(t)	
23MoZr	23.13	110	8.8	ZrO_2(t); $Zr(MoO_4)_2$	
28MoZr	27.97	90	13.0	ZrO_2(t); $Zr(MoO_4)_2$	
32MoZr	32.47	79	17.2	ZrO_2(t); $Zr(MoO_4)_2$	
58MoZr	58.52	23		$Zr(MoO_4)_2$	
68MoZr	67.67	1		$Zr(MoO_4)_2$; MoO_3	
100MoZr	100	2		MoO_3	

[a] Calculated volume fraction of monoclinic ZrO_2. From ref 19: $V_m = 1.311X_m/(1 + 0.311X_m)$; $X_m = (I(-111)_m + I(111)_m)/(I(-111)_m + I(111)_m + I(101)_t)$.

Results and Discussion

BET Surface Areas Measurements. Table 1 reports the chemical composition of the *x*MoZr catalysts prepared and their BET surface areas. The results show that the surface area increased from 26 to 131−143 $m^2\ g^{-1}$ with increasing Mo content up to 15−17 wt % MoO_3 (4.4−5.3 Mo atom/nm^2). For higher molybdenum loading, a significant decrease in the surface was observed. Similar behavior was reported for MoO_3−ZrO_2 catalysts prepared by different methods.[15,16] It should be noted, however, that for a given composition and calcination temperature, the sol−gel method used in the present study led to catalysts exhibiting large surface areas, compared with catalysts prepared by other methods such as impregnation, coprecipitation, mechanical mixing, or a different sol−gel method.[11,13,15,17] The Mo surface-density values corresponding to maximum surface area (see Table 1) agree with the estimated dispersion capacity of Mo(VI) species on the surface of tetragonal ZrO_2.[18]

Structure of Catalysts. *X-ray Diffraction (XRD).* Figure 1 shows the XRD patterns for the *x*MoZr series. The Bragg angle range shown (2θ between 20 and 40°) contains the most intense diffraction lines, which allow for the identification of various phases. Pure zirconia (0MoZr, not shown) and samples with low molybdenum loading (1−6% MoO_3) showed diffraction lines corresponding to tetragonal and monoclinic ZrO_2 phases. For higher Mo content, only the tetragonal phase was detected. From the intensity of diffraction lines corresponding with the (−111) and (111) planes of the monoclinic phase (2θ = 28.2 and 31.5°, respectively) and (101) of the tetragonal phase (2θ = 30.2°), the volume fraction of monoclinic phase can be inferred.[19] The results shown in Table 1 clearly indicate a progressive stabilization

(14) Onfroy, T.; Clet, G.; Houalla, M. *Microporous Mesoporous Mater.* **2005**, *82*, 99.
(15) Calafat, A.; Avilán, L.; Aldana, J. *Appl. Catal., A* **2000**, *201*, 215.
(16) Afanasiev, P. *Mater. Chem. Phys.* **1997**, *47*, 231.
(17) Chen, K.; Xie, S.; Iglesia, E.; Bell, A. T. *J. Catal.* **2000**, *189*, 421.
(18) Liu, Z.; Chen, Y. *J. Catal.* **1998**, *177*, 314.

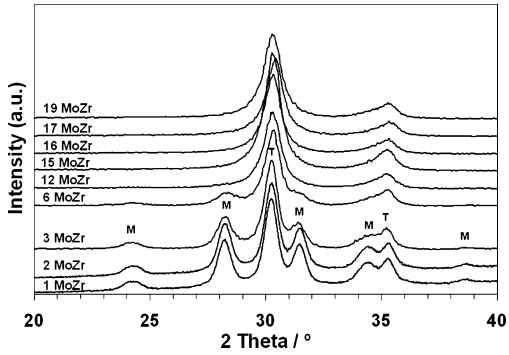

Figure 1. XRD patterns of MoO_3-ZrO_2 samples (1−19 wt % MoO_3). Characteristic diffraction peaks of tetragonal ZrO_2, T; monoclinic ZrO_2, M.

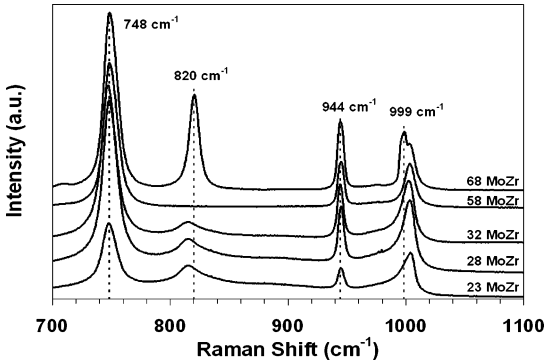

Figure 2. Raman spectra under ambient conditions of MoO_3-ZrO_2 samples (23−68 wt % MoO_3).

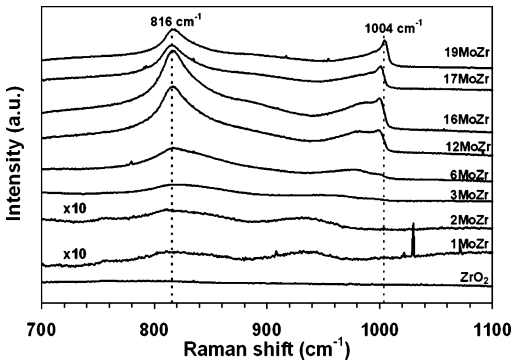

Figure 3. Raman spectra under ambient conditions of ZrO_2 and MoO_3-ZrO_2 samples (1−19 wt % MoO_3).

of the tetragonal form of zirconia with increasing Mo content. No diffraction lines attributable to crystalline molybdenum-containing phases were detected for Mo loading up to 19 wt % MoO_3. For higher Mo content, the XRD patterns showed, in addition to the lines corresponding to the tetragonal form of ZrO_2, peaks at $2\theta = 23.2$, 30.5, 35.4, and 38.7°, which can be assigned, respectively, to (112), (300) and (004), (220) and (114), and (222) diffraction lines of the $Zr(MoO_4)_2$ phase. The intensity of these lines increased with increasing Mo content up to 58 wt % MoO_3, and samples progressively showed smaller surface areas. The XRD pattern of the 58MoZr solid exhibited only the diffraction lines ascribed to $Zr(MoO_4)_2$. For higher Mo loading (68MoZr sample), the diffraction lines characteristic of crystalline MoO_3 were evidenced.

Raman and Infrared Spectroscopies. To examine the molecular structure of the catalysts and the presence of different phases, we examined samples by Raman spectroscopy under ambient conditions. Active Raman bands characteristic of monoclinic or tetragonal ZrO_2 appeared in the 100−650 cm^{-1} region. Tetragonal ZrO_2 gives rise to six Raman bands centered at 145, 268, 314, 463, 604 (shoulder), and 639 cm^{-1}.[20] A more complex spectrum is expected for monoclinic ZrO_2, which exhibits 18 Raman-active bands.[20] 0MoZr showed the above-mentioned bands characteristic of tetragonal ZrO_2 and other bands located at 104, 180, 192, 223, 337, 348, 382, 476, 502, 538, 559, and 617 cm^{-1}, which were assigned to monoclinic ZrO_2.[21] The relative intensity of the Raman bands points to an increase in the ZrO_2 tetragonal fraction with Mo addition, in agreement with XRD results. However, analysis of the Raman spectra of 12MoZr and 16MoZr samples indicated the presence of a minor amount of monoclinic ZrO_2, which was not observed by XRD. For higher Mo content, only the tetragonal form of ZrO_2 was detected.

On the other hand, the 700−1100 cm^{-1} zone of Raman spectra can yield information concerning the structure of Mo(VI) species. Figure 2 shows the Raman spectra of catalysts with high molybdenum content. Catalysts from 23MoZr to 58MoZr show a well-defined pattern consisting of three bands at 748, 944, and 1004 cm^{-1} that can be assigned to υ_{sym}(O−Mo−O), υ_{ant}(O−Mo−O), and υ(Mo═O) of $Zr(MoO_4)_2$.[22] Note that these were the only bands detected in the spectrum of 58MoZr, in agreement with XRD results. The spectrum for the 68MoZr solid shows, in addition to the bands assigned to $Zr(MoO_4)_2$, peaks at 820 and 999 cm^{-1}, which can be attributed, respectively, to O−Mo−O and Mo═O of crystalline MoO_3.[22]

The appearance of Raman spectra of samples with an MoO_3 content up to 19 wt % (Figure 3) differs from that of samples with higher molybdenum content (Figure 2). Now, broad bands at 780−880 and 900−1010 cm^{-1} are visible, indicating the coexistence of different Mo(VI) molecular species on the surface. Samples up to 6MoZr show a main band with a maximum at 816 cm^{-1} that can be assigned to the υ_{ant}(Mo−O−Zr) mode and which indicates that the molybdenum species are mainly interacting with ZrO_2 in these catalysts.[22] This band is asymmetric, showing Raman shifts at higher wavenumbers that can be related to the υ_{ant}(Mo−O−Mo) of surface polymolybdates.[17] The corresponding υ(Mo═O) for these species appears in the zone 900−1010 cm^{-1}; the maximum of this broad peak displaces at higher wavenumbers (up to ca. 980 cm^{-1}) when the molybdenum content in the sample increases from 1MoZr to 6MoZr (Figure 3). It was reported that the presence of water produces a decrease in the υ(Mo═O) Raman shift, whereas the latter increases with an increasing size of polymolybdate cluster.[17,23,24] In our case, the spectra were

(19) Toraya, H.; Yoshimura, M.; Somiya, S. *J. Am. Ceram. Soc.* **1984**, *67*, C119.
(20) Fernández López, E.; Sanchez Escribano, V.; Panizza, M.; Carnasciali, M. M.; Busca, G. *J. Mater. Chem.* **2001**, *11*, 1891.
(21) Valmalette, J. Ch.; Isa, M. *Chem. Mater.* **2002**, *14*, 5098.
(22) Xie, S.; Chen, K.; Bell, A. T.; Iglesia, E. *J. Phys. Chem. B* **2000**, *104*, 10059.
(23) Jezlorowski, H.; Knözinger, H. *J. Phys. Chem.* **1979**, *83*, 1166.

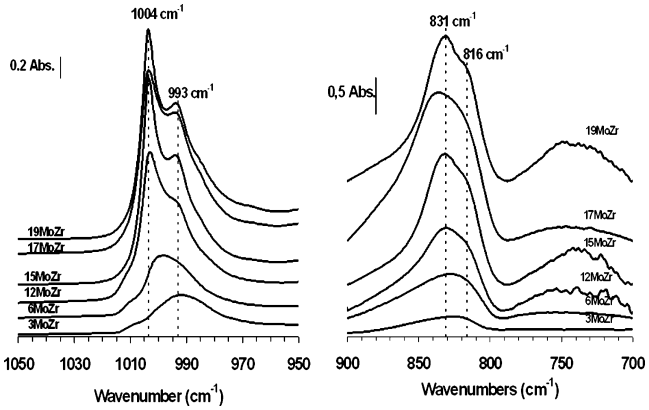

Figure 4. FTIR spectra of MoO_3-ZrO_2 samples (3−19 wt % MoO_3).

taken under ambient conditions after a treatment at 873 K. Thus, the displacement can be reasonably assigned to an increase in the size of polymeric molybdate species with increasing molybdenum content of samples.

The Raman spectra of the samples from 12MoZr to 19MoZr show a progressive development of well-defined maxima at 816 and 1000−1004 cm^{-1} (Figure 3). These bands can be assigned to tetragonal−pyramidal O═MoO_4 species interacting with the ZrO_2 surface via four Mo−O−Zr linkages (υ(Mo═O) = 1004 cm^{-1}, υ_{ant}(Mo−O−Zr) = 816 cm^{-1}).[22] These isolated tetragonal−pyramidal species are also present in samples with a higher molybdenum content (see spectra from 23MoZr to 32MoZr in Figure 2).

IR spectra (1000−700 cm^{-1} region) of the in situ treated samples yield additional information concerning the molecular structure of the Mo(VI) species. Only the spectra of samples up to 19MoZr are shown in Figure 4 because of the low transmittance of Mo-rich samples. The analysis of the υ(Mo═O) zone shows well-defined bands. For low molybdenum content, only one band is visible, centered at 993 cm^{-1} for 3MoZr and at 998 cm^{-1} for 6MoZr. Spectra of samples with higher Mo content (12−28 wt % MoO_3) display two bands at 1004 and 993 cm^{-1}. The intensity of both bands increases with an increase in molybdenum content at least up to 19MoZr (Figure 4). These results point to the progressive formation of tetragonal−pyramidal O═MoO_4 species (υ(Mo═O) at 1004 cm^{-1}) and polymolybdate species (υ(Mo═O) at 993 cm^{-1}) with increasing molybdenum content. Moreover, IR spectroscopy also allows for the analysis of υ_{ant}(M−O−M) bands associated with polymeric species, the intensity of which are expected to be higher in the infrared than in the Raman spectra.[25] In addition to the band at 816 cm^{-1} assigned to υ_{ant}(Mo−O−Zr), a band at 831 cm^{-1} attributed, from Raman results, to υ_{ant}(Mo−O−Mo) of octahedral polymolybdates[22] clearly developed (Figure 4). The intensity of this band increases with increasing molybdenum content up to the 19MoZr sample, which is consistent with the progressive formation of surface polymolybdate species.

UV−Vis Spectroscopy (DRS). Information concerning the environment of Mo(VI) can also be derived from the absorption edge energy values determined from UV−vis

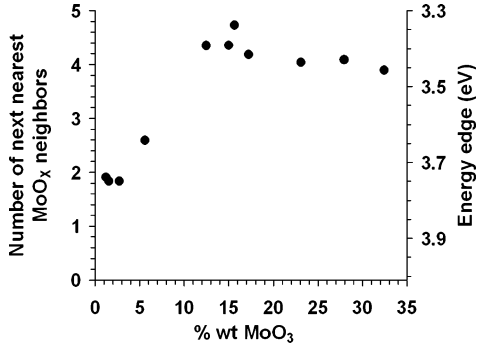

Figure 5. Absorption edge energy of MoO_3-ZrO_2 samples related to the number of next-nearest MoO_x neighbors as a function of the MoO_3 content.

Table 2. Absorption Edge Energy Determined for Some Mo(VI) Standard Compounds

standard	absorption edge energy (eV)	no. of MoO_x neighbors
MoO_3	3.12	6
$(NH_4)_6Mo_7O_{24}\cdot 4H_2O$	3.51	4
$CaMoO_4$	3.98	0

absorption spectra of the solids. The methodology involves a plot of $[F(R_\infty)h\nu]^2$ vs $h\nu$ where $F(R_\infty)$ is the Kubelka−Munk function and $h\nu$ the energy of the incident photon. The intercept of a linear fit of $[F(R_\infty)h\nu]^2$ yields the values of absorption edge energies. A direct relationship has been shown between the number of nearest MoO_x neighbors in crystalline MoO_x standards and the absorption edge energy value estimated by this formalism.[26,27] Table 2 shows the absorption edge energy values found for some Mo(VI) standard compounds and their number of nearest MoO_x neighbors. The absorption edge energies obtained for *x*MoZr samples are plotted in Figure 5 as function of MoO_3 content. The corresponding number of nearest MoO_x neighbors calculated from the results of Table 2 are also included in Figure 5. For Mo content up to 3.3 Mo atom/nm^2 (from 1MoZr to 6MoZr samples), high values of edge energies, which correspond to a low number of neighbors, were found. Further increases in the molybdenum content from 12 to 32 wt % MoO_3 yield edge energy values around 3.4 eV, which corresponds to ca. 4 nearest MoO_x neighbors according to the presence of polymolybdates in these samples. Note that the 58MoZr sample exhibited the highest absorption edge energy, 3.98 eV, which corresponded to the absence of MoO_x neighbors and coincided with the value obtained for the standard $CaMoO_4$ (Table 2). This is consistent with the predominant presence of the $Zr(MoO_4)_2$ phase evidenced by XRD and Raman spectroscopy.

Development of the Acidity with Mo Content. The development of the acidity of materials on Mo addition was monitored by adsorption of a probe molecule followed by infrared spectroscopy.

Lutidine was shown to be an appropriate probe for the detection of Brönsted and Lewis acid sites.[14,28,29] The location of the υ_{8a} and υ_{8b} bands of the aromatic ring is indicative of

(24) Chan, S. S.; Wachs, I. E.; Murrell, L. L.; Wang, L.; Hall, W. K. *J. Phys. Chem.* **1984**, *88*, 5831.
(25) Busca, G. *J. Raman Spectrosc.* **2002**, *33*, 348.
(26) Weber, R. S. *J. Catal.* **1995**, *151*, 470.
(27) Barton, D. G.; Shtein, M.; Wilson, R. D.; Soled, S. L.; Iglesia, E. *J. Phys. Chem. B* **1999**, *103*, 630.
(28) Jacobs, P. A.; Heylen, C. F. *J. Catal.* **1974**, *34*, 267.
(29) Corma, A.; Rodellas, C.; Fornes, V. *J. Catal.* **1984**, *88*, 374.

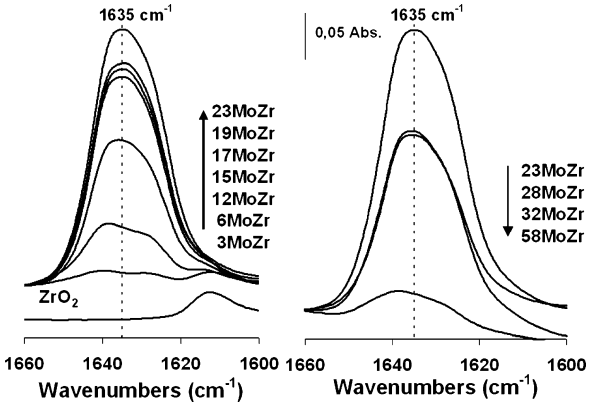

Figure 6. FTIR spectra of MoO_3-ZrO_2 samples after lutidine desorption at 423 K.

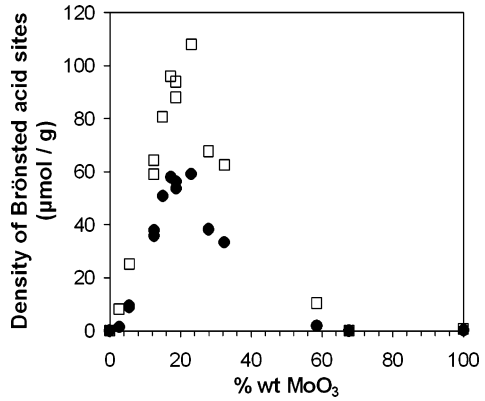

Figure 7. Density of adsorbed lutidine onto MoO_3-ZrO_2 samples vs molybdenum content. Empty symbols, adsorbed lutidine after desorption at 423 K; full symbols, adsorbed lutidine after desorption at 523 K.

the adsorption acid sites on surface. Moreover, the integrated molar absorption coefficients for the protonation and coordination of lutidine onto zirconia and zirconia-supported metal oxides allows for the quantification of these acid centers.[14] Figure 6 shows IR spectra of samples following lutidine adsorption at 373 K and consequent desorption at 423 K. Only the 1660−1600 cm^{-1} range is depicted because it includes the most significant IR bands. As expected, lutidine adsorbed on zirconia gave rise to peaks only at 1581 and 1612 cm^{-1}, which are attributed to its adsorption on Lewis acid sites (the former is not shown in the figure). Samples with low molybdenum content (3MoZr and 6MoZr) also showed peaks due to lutidine adsorbed on Lewis centers (1581 and 1612 cm^{-1} for 3MoZr and 1615 cm^{-1} for 6MoZr). The spectra indicated that the fraction of the total acid sites that represented Lewis acid sites is low and it decreased with an increase in molybdenum content.

The main feature of the spectra for molybdenum-containing samples is the presence of a broad band centered at 1635 cm^{-1}, which is due to the combination of υ_{8a} and υ_{8b} bands and is assigned to the presence of Brönsted acid sites.[14] For 3MoZr and 6MoZr, two maxima at 1640 and 1630 cm^{-1} are distinguished. The density of Brönsted acid sites (μmol/g) after desorption at 423 and 523 K, calculated as is indicated in the Experimental Section, is plotted in Figure 7 as a function of the MoO_3 content. For both desorption temperatures, the density (μmol/g) sharply increased with Mo content up to ca. 20 wt % MoO_3 and then decreased for higher loadings.

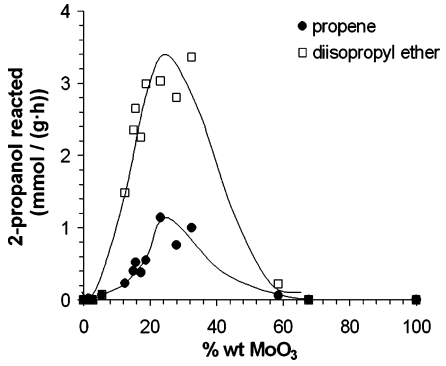

Figure 8. 2-Propanol reacted to propene or diisopropyl ether vs MoO_3 content. Reaction conditions $T = 353$ K, $P_{2-propanol} = 1.2$ kPa, GSHV = 5400 h^{-1}.

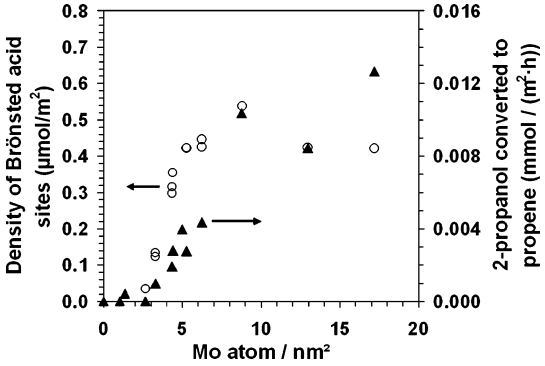

Figure 9. Density of Brönsted acid sites determined by adsorbed lutidine after desorption at 523 K (○) and rate of 2-propanol converted to propene (▲) per unit of surface area vs molybdenum surface density. Reaction conditions $T = 353$ K $P_{2-propanol} = 1.2$ kPa, GSHV = 5400 h^{-1}.

Development of the Catalytic Activity with Molybdenum Content. To gain further insight into the surface acidity, the catalytic properties of samples in an acid-catalyzed reaction (2-propanol transformation under Ar at 353 K) were studied. Only the dehydration products propene and diisopropyl ether were obtained. Figure 8 displays the catalytic activity per gram of sample vs molybdenum content. Samples 1MoZr and 2MoZr were not active under the experimental conditions used in the reaction test. An increase on the molybdenum content up to 20−25 wt % MoO_3 yields an increase on the production rate of both propene and diisopropyl ether. Note that pure MoO_3, 58MoZr, and 68MoZr showed negligible catalytic activity.

The decomposition of 2-propanol to propene has been directly related to the presence and abundance of relatively strong Brönsted acid sites (determined by lutidine adsorption) on WO_3/ZrO_2 and Nb_2O_5/ZrO_2 samples.[30,31]

Surface Structure/Acidity/Catalytic Activity Relationship. To account for the large variation in the surface of the solids, we plotted the surface density of Brönsted acid sites and the rate of 2-propanol converted to propene per unit surface vs Mo density (Mo atom/nm^2) in Figure 9. The results clearly show an abrupt increase in the surface density of relatively strong Brönsted acid sites (Brönsted acid sites that retain lutidine after desorption at 523 K) above ca. 3 atoms/nm^2. This suggests that a minimum of Mo surface density is required for the development of this acidity. The surface

(30) Onfroy, T.; Clet, G.; Houalla, M. *J. Phys. Chem. B* **2005**, *109*, 3345.
(31) Onfroy, T.; Clet, G.; Houalla, M. *J. Phys. Chem. B* **2005**, *109*, 14588.

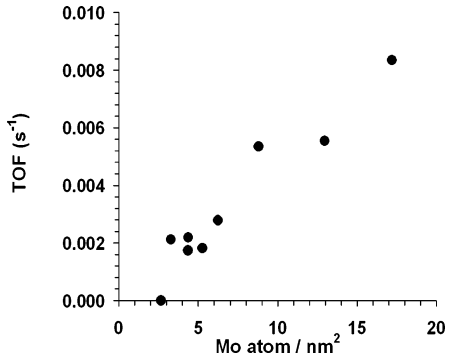

Figure 10. TOF of 2-propanol dehydration to propene referred to acid centers determined by lutidine adsorption vs molybdenum surface density. Acid centers determined after lutidine desorption at 523 K. Reaction conditions $T = 353$ K $P_{2-\text{propanol}} = 1.2$ kPa, GSHV $= 5400$ h^{-1}.

density of these sites increased with Mo surface density up to 5−6 Mo atom/nm^2 and then leveled off for higher loading up to 17 Mo atom/nm^2. These results, and those relative to the structure exposed above, indicate that the development of relatively strong Brönsted acid sites for Mo surface density ≥ 3 atom/nm^2 can be associated with the formation of polymolybdate species, as was demonstrated by Raman, UV−vis (RDS), and FTIR experiments. For MoO_3 content higher than 20 wt %, polymolybdates species coexist with $Zr(MoO_4)_2$, as was shown by Raman and XRD experiments. Although the BET surface area simultaneously decreases because of the formation of $Zr(MoO_4)_2$, polymolybdate species remain dispersed on the surface and the number of strong Brönsted acid sites per unit surface area appears little affected by the increase in molybdenum content.

Figure 9 also shows that the rate of propene formation increases with the molybdenum surface density. However, the increase is sharper for values of molybdenum density that are lower than the accepted monolayer value (5−6 Mo atom/nm^2). Analysis of the results of Figure 9 indicates a good correlation between the abundance of relatively strong Brönsted acid sites, determined by adsorption of lutidine and desorption at 523 K, and the propene formation. Similar correlations have already been reported for other solid acids on the basis of supported metal oxide systems.[30,31]

Assuming that the abundance of Brönsted acid sites is directly related to the propene formation, it would be of interest to investigate the evolution of their relative activity with molybdenum content. One can thus define a turnover frequency (TOF) expressing the activity in the 2-propanol transformed to propene per relatively strong Brönsted acid site. Figure 10 shows the variation in TOF with the molybdenum surface density. Note that meaningful TOFs were measured only for solids containing more than 3 Mo atom/nm^2. A sharp increase in the TOF values with increasing molybdenum surface density up to monolayer values (5−6 Mo atom/nm^2) was observed, followed by a more progressive increase up to the 32MoZr sample.

These results are consistent with the development of new Brönsted acid sites that exhibit progressively higher intrinsic activity for the dehydration of 2-propanol, with increasing molybdenum content up to 32 wt/wt MoO_3 (molybdenum density ca. 20 Mo atom/nm^2).

Acknowledgment. We thank MCYT (MAT2002-01739, MAT2005-03456) and CIRIT (2005-SGR00184) for financial support.

CM052433C